Coupled quasidiabatic potential energy surfaces for LiFH

Ahren W. Jasper, Michael D. Hack, and Donald G. Truhlar[a)]
Department of Chemistry and Supercomputer Institute, University of Minnesota, Minneapolis, Minnesota 55455

Piotr Piecuch[b)]
Department of Chemistry, Michigan State University, East Lansing, Michigan 48824

(Received 2 November 2001; accepted 31 January 2002)

We present high-level *ab initio* calculations for the global adiabatic potential energy surfaces of the ground state ($\tilde{X}\,^2A'$) and several excited states ($\tilde{A}\,^2A'$, $\tilde{B}\,^2A''$, $\tilde{C}\,^2A'$, $\tilde{D}\,^2A'$, and $\tilde{E}\,^2A''$) of LiFH, including the valleys leading to Li+HF and LiF+H. The *ab initio* calculations were carried out using the multireference singles and doubles configuration interaction method with 99 reference configuration state functions (CSFs) for the $^2A'$ states and 39 reference CSFs for the $^2A''$ states. The basis set consisted of 140 contracted Gaussian functions, including specifically optimized diffuse functions, and calculations were performed on a dense grid of $\sim$3500 nuclear geometries which allowed us to construct an accurate analytic representation of the two lowest-energy LiFH potential energy surfaces. An analytic 2×2 quasidiabatic potential energy matrix was obtained by fitting physically motivated functional forms to the *ab initio* data for the two lowest-energy adiabatic states and explicitly including long-range interactions. The newly presented LiFH fit is compared to several ground-state LiFH fits and one excited-state LiFH fit that have appeared in the literature. © *2002 American Institute of Physics.*
[DOI: 10.1063/1.1463440]

I. INTRODUCTION

The LiFH system is ideal for detailed theoretical study because it is relatively simple, yet features an interesting potential energy surface topography. The ground-state LiFH potential energy surface[1–13] and the dynamics of the electronically adiabatic Li+HF→LiF+H reaction[10–25] have been widely studied. The excited states[8,26,27] and electronically nonadiabatic dynamics[26,28] of LiFH have attracted attention only recently. The ground-state potential energy surface has a relatively deep van der Waals well in the Li($2s$)+HF entrance valley and a barrier in the LiF+H exit valley. A strongly bound excited-state complex (exciplex) is present in the first excited state at a geometry similar to (but tighter than) the geometry of the ground-state van der Waals well. The ground- and first-excited states of the LiFH system are coupled nonadiabatically, forming a seam of avoided crossing at larger Li–F and H–F separations.

The features of the coupled LiFH potential energy surfaces allow for interesting dynamical processes. For example, the ground-state van der Waals molecules (Li···FH) may be excited into the exciplex [(Li···FH)*]. These excited-state complexes are relatively long-lived and may undergo electronically nonadiabatic dissociation[26,28] which can proceed either reactively to form LiF+H or nonreactively to form electronically quenched Li($2s$)+HF

$$\mathrm{Li}\cdots\mathrm{FH}\xrightarrow{h\nu}(\mathrm{Li}\cdots\mathrm{FH})^*\rightarrow\begin{cases}\mathrm{LiF}+\mathrm{H} & \text{(R1a)}\\ \mathrm{Li}(2s)+\mathrm{HF}. & \text{(R1b)}\end{cases}$$

This type of reaction is of particular importance as a means of probing the transition state region of the excited-state Li($2p$)+HF reaction. For sufficiently large excitation energies $h\nu$, another dissociation pathway is accessible where the (Li···FH)* exciplexes dissociate in an electronically excited state and form the Li($2p$)+HF product.

In order to facilitate the detailed theoretical study of the LiFH system, we present high-level *ab initio* calculations for a dense grid of nuclear geometries for the ground state and first five excited states of LiFH. Some of the features on the ground- and excited-state adiabatic potential surfaces are the result of the interaction of covalent and ionic valence bond configurations, and a multiconfigurational treatment is necessary to accurately describe these features. *Ab initio* calculations were performed with the multireference configuration interaction (MRCI) method employing relatively large reference spaces and a large one-electron basis set. Although in this work we focus mainly on the potential energy surfaces of the ground- and first-excited states of the LiFH system, we also present less extensive results for other low-lying states of LiFH, including all states that correlate with the Li($2s\,^2S$)+HF($X\,^1\Sigma^+$) and Li($2p\,^2P$)+HF($X\,^1\Sigma^+$) limits.

The energies obtained from the *ab initio* calculations were used to construct a three-dimensional analytic fit for the two lowest-energy quasidiabatic[29–44] states of LiFH and their electronic coupling. In a previous work,[26] we have presented semiclassical trajectory photodissociation calculations using analytic fits for the NaFH and LiFH systems. The LiFH fit used in the previous study (which may be called surface fit H) was based on a limited set of *ab initio* data. In the current work, we describe an improved LiFH fit called surface fit J

a)Electronic mail: truhlar@umn.edu
b)Selected as an Alfred P. Sloan Research Fellow in 2002.

TABLE I. Calculated (MRDCI) and experimental (Expt.) excitation energies and ionization potentials (IP) of Li (in eV).

	MRDCI	Expt.[a]
$2s\ ^2S \rightarrow 2p\ ^2P$	1.837	1.848
$2s\ ^2S \rightarrow 3s\ ^2S$	3.373	3.373
$2s\ ^2S \rightarrow 3p\ ^2P$	3.833	3.834
IP	5.372	5.392

[a]Reference 74.

TABLE II. Calculated (MRDCI) and experimental (Expt.) electron affinities of F and H (in eV).

	MRDCI	Expt.[a]
F	3.31	3.40
H	0.74	0.75

[a]Reference 72.

that is based on the larger set of *ab initio* data presented here. Care has also been taken to explicitly include accurate long-range interactions, which were not included in the preliminary fit. The newly presented LiFH quasidiabatic potential energy matrix is global and can be used to describe ground-state or nonadiabatic bimolecular scattering processes as well as the photodissociation processes shown in Eqs. (R1a) and (R1b) for both quantum-mechanical and semiclassical dynamics simulations.

In Sec. II we present the details of the *ab initio* calculations for the LiFH system. Section III describes the procedure we used to obtain an analytic fit of the *ab initio* data. Section IV discusses the fit and compares it to several ground-state LiFH fits and one excited-state LiFH fit that have appeared previously in the literature.[4,5,8,11–13]

II. *AB INITIO* ELECTRONIC STRUCTURE CALCULATIONS

Ab initio calculations were performed using the MRDCI variant[45] of the multireference configuration interaction (MRCI) method. In this approach, a series of variational CI calculations is carried out using sets of spin- and symmetry-adapted configuration state functions (CSFs) that are selected from all possible CSFs generated by single and double substitutions in reference configurations. For multireference calculations, the reference space contains those CSFs that are believed to be essential for the description of the nondynamical correlation in the electronic states of interest, as well as some of the leading configurations needed for dynamical correlation. In each CI calculation, the selection of excited CSFs is made based on their importance in the CI wave function expansions, as determined by a selection threshold T (usually, a few μE_h or a fraction of one μE_h). The selection of excited CSFs is based on the estimated energy lowering effect of each added CSF on the desired eigenvalues of the Hamiltonian matrix involving reference CSFs, as explained elsewhere.[45] The CI eigenvalue problem then is solved several times for different values of selection threshold T, and the resulting energies are extrapolated to the $T=0$ limit. This limit corresponds to the complete MRCISD (MRCI singles and doubles) eigenvalue problem.[45] The final MRDCI energy of a given electronic state is obtained by adding the simplified quasidegenerate Davidson correction[46] to the extrapolated MRCISD energy. In each of the three types of the MRDCI calculations reported in this work (referred to as strategies A–C and fully described below), the extrapolated energies were obtained using three threshold values T, as described below.

Although in this study we were mainly interested in the two lowest states of $^2A'$ symmetry, we also wanted to understand the topography of the potential energy surfaces characterizing other low-lying states of the LiFH system. Thus, along with the ground state ($\tilde{X}\ ^2A'$) and the first excited state ($\tilde{A}\ ^2A'$), we calculated the potential energy surfaces of four other states, including two more states of the $^2A'$ symmetry (the $\tilde{C}\ ^2A'$ and $\tilde{D}\ ^2A'$ states) and the two lowest states of $^2A''$ symmetry (the $\tilde{B}\ ^2A''$ and $\tilde{E}\ ^2A''$ states). The calculated states correlate with the six doublet states corresponding to the lowest-energy noninteracting-atom limit [i.e., the $\mathrm{Li}(2s\ ^2S)+\mathrm{F}(2p^5\ ^2P)+\mathrm{H}(1s\ ^2S)$ asymptote]. These states include the $\mathrm{Li}(2s\ ^2S, 2p\ ^2P, 3s\ ^2S)+\mathrm{HF}(X\ ^1\Sigma^+)$ states of the reactants and the $\mathrm{LiF}(X\ ^1\Sigma^+, A\ ^1\Pi, B\ ^3\Pi, C\ ^3\Sigma^+, D\ ^1\Sigma^+)+\mathrm{H}(1s\ ^2S)$ states of products. In choosing the reference spaces and basis sets for

TABLE III. Ground-state properties of HF, LiF, and LiH. A comparison of the calculated (MRDCI) and experimental (Expt.) data.

	r_e/Å[a]		ω_e/cm^{-1}[b]		D_0/eV[c]		μ/D[d]		ΔE/eV[e]	
Diatom	MRDCI	Expt.[f]	MRDCI	Expt.[f]	MRDCI	Expt.[f]	MRDCI	Expt.[f,g]	MRDCI	Expt.[h]
HF	0.9165	0.9168	4147.7	4138.3	5.68	5.87	1.819	1.826	0.00	0.00
LiF	1.5645	1.5639	903.7	910.3	5.67	5.91	6.358	6.325	0.21	0.17
LiH	1.5946	1.5957	1402.0	1405.7	2.44	2.43	5.851	5.882	3.37	3.60

[a]The equilibrium bond length.
[b]The harmonic vibrational frequency.
[c]The dissociation energy. The MRDCI value of D_0 was calculated from $D_e-\omega_e/2$, where D_e is a difference between the asymptotic ($r=7.5\,a_0$ for HF, $r=31\,a_0$ for LiF, and $r=15\,a_0$ for LiH) and equilibrium values of the MRDCI ground-state energies.
[d]The dipole moment.
[e]The difference between the energy of the diatom at its equilibrium bond length and the energy of the Li+HF asymptote at the HF equilibrium bond length.
[f]Reference 75.
[g]Average value for the ground vibrational state.
[h]Computed from D_0 and ω_e.

TABLE IV. Vertical excitation energies (in eV) from the $X\ ^1\Sigma^+$ state of HF at the experimental equilibrium distance $r_e=0.917$ Å. Continuous absorption starting at 60 600 cm^{-1} (7.51 eV) has been attributed to the $X\ ^1\Sigma^+ \rightarrow {}^1\Pi$ transition (Ref. 75 and references therein).

State[a]	MRDCI[b]	MRDCI[c]
$^3\Pi$	10.060	10.06
$^1\Pi$	10.417	10.41
$^3\Sigma^+$	13.442	13.59

[a]Lowest excited state for each symmetry.
[b]Present work, $[5s4p3d2\,f/5s4p2d]$ basis set.
[c]Reference 76, $[7s5p2d/3s1p]$ basis set.

our MRDCI calculations, we obtain a balanced description of the four lowest $^2A'$ and two lowest $^2A''$ states. We also obtain a very accurate description of the lowest two $^2A'$ states, and this was used to construct a 2×2 quasidiabatic fit described in Secs. III and IV.

The basis set used in the MRDCI calculations consisted of the standard 6-311G($3d2f$,$3p2d$) basis set,[47] augmented by several diffuse functions whose exponents were optimized to accurately reproduce selected properties of the Li, H, and F atoms (excitation energies of Li, ionization potential of Li, and electron affinities of H and F) and basic properties of the HF, LiF, and LiH diatomic fragments (the equilibrium bond lengths, vibrational term values, dissociation energies, dipole moments, and low-lying excited states). The following diffuse functions were used to augment the 6-311G($3d2f$,$3p2d$) basis set (exponents in parentheses): $s(0.0052)$ and $p(0.0097)$ functions centered on Li, $s(0.089)$, $s(0.000\,01)$, and $p(0.083)$ functions centered on F, and $s(0.037)$, $s(0.012)$, and $p(0.055)$ functions centered on H. Cartesian representations of the d and f functions were employed throughout, so that the total number of contracted Gaussian functions in the basis set was 140. The high accuracy of our basis set can be judged by the results of the MRDCI calculations for the Li, H, and F atoms and HF, LiF, and LiH molecules, as shown in Tables I–VI. The total absolute energies for the diatomic calculations at the minimum energy bond length are $-100.353\,263$, $-107.298\,414$, and $-8.043\,992\ E_h$, for the HF, LiF, and LiH diatomics, respectively.

The MRDCI calculations reported in this work were performed using ground-state restricted open-shell Hartree-Fock (ROHF) orbitals, and the lowest $1a'$ molecular orbital was kept frozen. All ROHF and correlated calculations were performed using the C_s symmetry common to all LiFH nuclear configurations. The use of C_s symmetry in our calculations

TABLE V. Vertical excitation energies (in eV) from the $X\ ^1\Sigma^+=1\ ^1\Sigma^+$ state of LiF at the experimental equilibrium distance $r_e=1.564$ Å. Peaks in the electron energy loss spectrum are at 6.6, 8.7, 10.9, 62.0 eV (Ref. 75).

State	MRDCI[a]
$1\ ^3\Pi$	6.58
$1\ ^1\Pi$	6.57
$1\ ^3\Sigma^+$	6.96
$2\ ^1\Sigma^+$	6.98

[a]Present work, $[5s4p3d2\,f/5s4p3d2\,f]$ basis set.

TABLE VI. Vertical excitation energies (in eV) from the $X\ ^1\Sigma^+=1\ ^1\Sigma^+$ state of LiH at the experimental equilibrium distance $r_e=1.595$ Å.

State	MRDCI[a]
$1\ ^3\Sigma^+$	3.27
$2\ ^1\Sigma^+$	3.62[b]
$1\ ^3\Pi$	4.25[c]
$1\ ^1\Pi$	4.26[d]

[a]Present work, $[5s4p3d2\,f/5s4p2d]$ basis set.
[b]The T_e (minimum to minimum) excitation energy is 3.29 eV. The experimental value of T_e is 3.29 eV (Ref. 75).
[c]The lowest stable $^3\Pi$ state is located at ~1700 cm^{-1} or 0.21 eV below the lowest stable $^1\Pi$ state.
[d]The T_e (minimum to minimum) excitation energy is 4.32 eV. The experimental value of T_e is 4.33 eV (Ref. 75).

prompts a few remarks. When collinear arrangements of the Li, F, and H atoms are approached (i.e., at Li–F–H angles of 180° or 0°), the symmetry of the LiFH electronic Hamiltonian increases from C_s to $C_{\infty v}$, so that the A' and A'' states classify as Σ, Π, etc. states (similarly, the ROHF orbitals that for the bent configurations classify as a' and a'' orbitals become σ, π, etc. orbitals for the collinear arrangements of the Li, F, and H atoms). The incomplete reference spaces and the CSF selection procedures that are used in MRDCI calculations give results that are not unitarily invariant with respect to general orbital rotations within the core, active, and virtual blocks. In particular, the results for the collinear geometries may depend on whether we use C_s or $C_{\infty v}$ symmetry-adapted orbitals and CSFs. For this reason, we never used the $C_{\infty v}$ symmetry (or its C_{2v} Abelian subgroup) in our calculations, as this would result in a nonsmooth behavior of our calculated potential energy surfaces for Li–F–H angles approaching 180° and 0°. To mimic the collinear arrangements of the Li, F, and H atoms, while retaining the C_s symmetry for all geometries, we included Li–F–H angles of 179.99° and 0.01° in our grids.

The MRDCI calculations for the $^2A'$ states are based on 62 symmetry-adapted reference configurations (as defined by the orbital occupation numbers) or, equivalently, 99 spin- and symmetry-adapted CSFs. The $^2A''$ states were described by 24 reference configurations or 39 CSFs. These configurations were chosen so as to provide an accurate and well balanced zero-order description of the four lowest $^2A'$ and two lowest $^2A''$ states in the 6-root calculations with thresholds $T=4$, 6, and 8 μE_h referred to as strategy A (see the discussion below for further details), over a wide range of nuclear geometries, including: the Li+HF and LiF+H dissociation channels, the vdW well on the ground-state potential energy surface, the excited-state well, the region of the avoided crossing between ground- and excited-state potential energy surfaces, and the transition-state region for the ground-state Li+HF→LiF+H reaction.

In the language appropriate for the Li+HF limit, the reference CSFs defining the $^2A'$ CI subproblem included the ground-state ROHF determinant, the $2s\rightarrow2p$, $3s$, $3p$, $3d$, $4s$, $4p$, etc. single excitations in Li (important to describe excited states of the Li···FH complex), the valence $\sigma\rightarrow\sigma^*$ single and double excitations in HF (important to describe the bond breaking in HF), the valence $\pi\rightarrow\sigma^*$ as well as the

Rydberg σ, $\pi\rightarrow\sigma$, π mono- and biexcitations in HF, the $2s(\mathrm{Li})\rightarrow\sigma^*(\mathrm{HF})$, $\sigma(\mathrm{HF})\rightarrow 2s$, $2p$, $3s$, $3p$, $3d$, $4s$, $4p(\mathrm{Li})$, etc. and $\pi(\mathrm{HF})\rightarrow 2s$, $2p$, $3s$, $3p$, $3d$, $4s$, $4p(\mathrm{Li})$, etc. monoexcitations between Li and HF, and various "product" double excitations, such as $\sigma^2(\mathrm{HF})\rightarrow 2s^1 2p^1$, $2s^1 3s^1(\mathrm{Li})$, $\sigma^2(\mathrm{HF})\rightarrow 2s^1(\mathrm{Li})(\sigma^*)^1(\mathrm{HF})$, $\pi^2(\mathrm{HF})\rightarrow 2s^1 2p^1$, $2s^1 3s^1(\mathrm{Li})$, and $\pi^2(\mathrm{HF})\rightarrow 2s^1(\mathrm{Li})(\sigma^*)^1(\mathrm{HF})$. Thus, along with the ground-state ROHF determinant

$$\Phi^{(0)}=|\{\mathrm{core}\}(4a')^2(5a')^2(1a'')^2(6a')^1|, \tag{1}$$

where $\{\mathrm{core}\}=(1a')^2(2a')^2(3a')^2$, in which the lowest $1a'$ molecular orbital ($\sim 1s$ orbital on fluorine) was kept frozen, the CSFs of the following types were chosen as reference configurations:

$$\Phi_n^{(1)}=|\{\mathrm{core}\}(4a')^2(5a')^2(1a'')^2(na')^1|, \tag{2}$$

$$\Phi_n^{(2)}=|\{\mathrm{core}\}(4a')^1(5a')^2(1a'')^2(6a')^1(na')^1|, \tag{3}$$

$$\Phi_n^{(3)}=|\{\mathrm{core}\}(4a')^2(5a')^1(1a'')^2(6a')^1(na')^1|, \tag{4}$$

where $7\leqslant n\leqslant 20$,

$$\Phi^{(4)}=|\{\mathrm{core}\}(4a')^1(5a')^2(1a'')^2(6a')^2|, \tag{5}$$

$$\Phi^{(5)}=|\{\mathrm{core}\}(4a')^2(5a')^1(1a'')^2(6a')^2|, \tag{6}$$

$$\Phi_n^{(6)}=|\{\mathrm{core}\}(5a')^2(1a'')^2(6a')^1(na')^2|, \tag{7}$$

$$\Phi_n^{(7)}=|\{\mathrm{core}\}(5a')^2(1a'')^2(6a')^2(na')^1|, \tag{8}$$

$$\Phi_n^{(8)}=|\{\mathrm{core}\}(4a')^2(1a'')^2(6a')^1(na')^2|, \tag{9}$$

$$\Phi_n^{(9)}=|\{\mathrm{core}\}(4a')^2(1a'')^2(6a')^2(na')^1|, \tag{10}$$

where $7\leqslant n\leqslant 9$, and

$$\Phi^{(10)}=|\{\mathrm{core}\}(4a')^2(5a')^2(1a'')^1(6a')^1(2a'')^1|, \tag{11}$$

$$\Phi_n^{(11)}=|\{\mathrm{core}\}(4a')^1(5a')^1(1a'')^2\times(6a')^1(7a')^1(na')^1|,$$

$$(n=31,32), \tag{12}$$

$$\Phi^{(12)}=|\{\mathrm{core}\}(4a')^1(5a')^2(1a'')^1\times(6a')^1(7a')^1(12a'')^1|, \tag{13}$$

$$\Phi^{(13)}=|\{\mathrm{core}\}(4a')^2(5a')^1(1a'')^1\times(6a')^1(7a')^1(12a'')^1|. \tag{14}$$

Two CSFs were particularly important for the description of the two lowest $^2A'$ states, namely, the ROHF configuration $\Phi^{(0)}$, Eq. (1), and the monoexcited configuration $\Phi_7^{(1)}$, Eq. (2). These two configurations correlate with the $\mathrm{Li}(2s\,^2S)+\mathrm{HF}(X\,^1\Sigma^+)$ and the $\mathrm{Li}(2p\,^2P)+\mathrm{HF}(X\,^1\Sigma^+)$ limits of reactants. In this case, the $6a'$ and $7a'$ orbitals represent, respectively, the $2s$ and $2p$ orbitals of Li. As the Li–F distance decreases and the H–F distance increases, the $7a'$ orbital evolves into an antibonding orbital of HF having a significant admixture of diffuse atomic orbitals centered on Li, allowing us to describe an ionic intermediate $\mathrm{Li}^+-(\mathrm{F–H})^-$, which plays an important role in the electron transfer between the excited lithium atom and the HF fragment in $(\mathrm{LiFH})^*$, ultimately allowing for nonadiabatic dissociation of $(\mathrm{LiFH})^*$ into the reaction products, Eq. (R1a). At the same time, the $6a'$ orbital becomes a $1s$ orbital of hydrogen, so that when the H–F bond finally breaks, the ROHF configuration $\Phi^{(0)}$, Eq. (1), describes the ionic product channel, i.e., $\mathrm{LiF}(X\,^1\Sigma^+)+\mathrm{H}(1s\,^2S)$. The presence of the carefully optimized diffuse functions in the basis set was essential for obtaining an accurate description of the $\tilde{X}\,^2A'$ and $\tilde{A}\,^2A'$ potential energy surfaces in the region of nuclear geometries where the nonadiabatic transitions and a significant rearrangement in the electronic structure of the excited $\mathrm{Li}\cdots\mathrm{FH}$ complex (from the covalent to largely ionic $\mathrm{Li}^+-(\mathrm{F–H})^-$ intermediate), which are responsible for the photoinduced charge transfer in $\mathrm{Li}\cdots\mathrm{FH}$, take place.

A similar set of references, including the $2s\rightarrow 2p$, $3p$, $3d$, $4p$, etc. single excitations in Li, the $\sigma\rightarrow\pi$ and $\pi\rightarrow\sigma^*$, σ, π single excitations in HF, and the $\sigma(\mathrm{HF})\rightarrow 2p$, $3p$, $3d$, $4p(\mathrm{Li})$, $\pi(\mathrm{HF})\rightarrow 2s$, $2p$, $3s$, $3p$, $3d$, $4s$, $4p(\mathrm{Li})$, $\sigma^2(\mathrm{HF})\rightarrow 2s^1 2p^1(\mathrm{Li})$, and $\pi^2(\mathrm{HF})\rightarrow 2s^1 2p^1(\mathrm{Li})$ intersystem excitations, was defined for the $^2A''$ states. Thus, along with the

$$\tilde{\Phi}_n^{(1)}=|\{\mathrm{core}\}(4a')^2(5a')^2(1a'')^2(na'')^1|, \tag{15}$$

$$\tilde{\Phi}_n^{(2)}=|\{\mathrm{core}\}(4a')^1(5a')^2(1a'')^2(6a')^1(na'')^1|, \tag{16}$$

and

$$\tilde{\Phi}_n^{(3)}=|\{\mathrm{core}\}(4a')^2(5a')^1(1a'')^2(6a')^1(na'')^1| \tag{17}$$

configurations, where $n=2-7$, we included in the reference space the

$$\tilde{\Phi}_n^{(4)}=|\{\mathrm{core}\}(4a')^2(5a')^2(1a'')^1(6a')^1(na')^1| \tag{18}$$

configurations with $n=7-9$, and the

$$\tilde{\Phi}^{(5)}=|\{\mathrm{core}\}(4a')^2(5a')^2(1a'')^1(6a')^2|, \tag{19}$$

$$\tilde{\Phi}^{(6)}=|\{\mathrm{core}\}(4a')^2(1a'')^2(6a')^2(2a'')^1|, \tag{20}$$

and

$$\tilde{\Phi}^{(7)}=|\{\mathrm{core}\}(5a')^2(1a'')^2(6a')^2(2a'')^1|, \tag{21}$$

configurations.

The above reference spaces do not represent complete model spaces. The fact that we did not use a complete active space approach, which would considerably increase the cost of our calculations, was compensated for by a careful choice

of reference configurations. These reference configurations were selected in such a way that they rotate into one another when the nuclear geometry varies. The appropriateness of our selection of references can be best illustrated by the size of the sum of the squared magnitudes of the coefficients of the above reference CSFs in the final CI wave function expansions of the four lowest $^2A'$ and two lowest $^2A''$ states defining strategy A, the two lowest $^2A'$ states defining strategy B, and the lowest $^2A'$ state defining strategy C (for the precise definitions of these strategies, see the next paragraph). For the majority of geometries considered in this study, these sums were greater than 0.95, and they were greater than 0.90 for all nuclear geometries and all computational strategies considered here.

As in our earlier study of the potential energy surfaces of the NaFH system,[34] the MRDCI calculations for LiFH were performed in three stages, with each successive stage employing a set of smaller selection thresholds T and a subset of geometries used in the earlier stage. Thus, the entire potential energy surfaces for the four lowest $^2A'$ and two lowest $^2A''$ states were first explored using the threshold values $T=4$, 6, and 8 μE_h. This initial 6-root calculation is referred to as strategy A. The exploratory calculations constituting strategy A were followed by more accurate calculations for the $\tilde{X}\,^2A'$ and $\tilde{A}\,^2A'$ states, and this 2-root calculation is referred to as strategy B. In these calculations, we used the smaller threshold values $T=1$, 2, and 3 μE_h. This set of calculations focused on the regions of potential energy surfaces critical for the dynamics of the nonadiabatic dissociation of the excited LiFH system, including the geometries along the Li+HF→LiF+H reaction path, the regions of the van der Waals minima on the $\tilde{X}\,^2A'$ and $\tilde{A}\,^2A'$ potential energy surfaces, the saddle-point region on the ground-state potential energy surface, and the region of the avoided crossing of the $\tilde{X}\,^2A'$ and $\tilde{A}\,^2A'$ states.

The final set of calculations, denoted as strategy C, employed the smallest selection thresholds, namely, $T=0.15$, 0.30, and 0.45 μE_h. In these most accurate calculations, performed only for the ground state, we focused on H–F distances not exceeding 2.6 a_0, i.e., on the shallow van der Waals minimum, the entire reactant valley, and the product valley up to the barrier for the Li+HF→LiF+H reaction. Strategy C was important for improving the description of the van der Waals well and the saddle-point region on the ground-state potential energy surface, which have also been examined by one of us with highly accurate coupled-cluster calculations.[13] In fact, we used the results of these coupled-cluster calculations to choose the optimum values of T for the MRDCI calculations defining strategies B and C.

As pointed out in our earlier study of the NaFH system,[34] the use of very small thresholds T, such as those defining strategy C, is essential to obtain the correct description of shallow minima on potential energy surfaces with the MRDCI method. For example, the estimated error of extrapolation to the $T=0$ limit of the complete MRCISD problem characterizing strategy C was 0.001–0.006 eV, which is a reasonable accuracy for the ground-state potential energy surface in that it is characterized by a van der Waals minimum located ~0.24 eV below the Li+HF asymptote. The other regions of the $\tilde{X}\,^2A'$ and $\tilde{A}\,^2A'$ potential energy surfaces are accurately described with strategy B, which has estimated extrapolation errors of 0.01–0.03 eV for all nuclear geometries included in the calculations. The least expensive set of calculations, defining strategy A, has extrapolation errors of 0.02–0.09 eV; this accuracy level was sufficient to provide information about the global topography of the potential energy surface of the four lowest $^2A'$ and two lowest $^2A''$ states, and information obtained in the 6-root strategy A calculation was useful for choosing the functional form for our analytic fit of the potential energy surfaces of the $\tilde{X}\,^2A'$ and $\tilde{A}\,^2A'$ states described in Secs. III and IV. The use of the above selection thresholds allowed us to substantially reduce the original dimension of the $^2A'$ MRCISD problem, from 23 616 292 CSFs for all single and double excitations to less than ~70 000 CSFs in the $T=4$, 6, 8 μE_h case, to less than ~100 000 CSFs in the $T=1$, 2, 3 μE_h case, and to less than ~200 000 CSFs in the $T=0.15$, 0.30, 0.45 μE_h case. The use of the three-step approach (strategies A–C) allowed us to reduce the cost of our calculations further, since we used more expensive strategies B and C primarily in the regions important for the dynamics. The regions of the LiFH potential energy surfaces (for example, regions characterized by very high energies) which cannot be accessed during the nonadiabatic dissociation of the excited Li···FH complex do not have to be treated as accurately as regions critical for the dynamics of this process. The use of strategies A–C and the use of the MRDCI scheme, which is based on selecting relatively small sets of CSFs out of large sets of CSFs corresponding to a complete MRCI problem, allowed us to cut down the cost of our calculations so much that the otherwise expensive MRCI calculations could be performed on dense grids of nuclear geometries involving several thousands of points in a reasonable amount of time. The results of the MRDCI calculations for each of the three strategies A–C for a wide range of nuclear geometries is available as supplementary information.[48] The *ab initio* energies are reported in the supplementary material relative to the zero of energy defined as the energy of the ground electronic state at $r_{LiF}=15.0\,a_0$, $r_{HF}=1.7325\,a_0$, and $\theta=179.99°$. The total absolute energies for the ground electronic state at this geometry are −107.803 247, −107.804 286, and −107.804 580 E_h for strategies A, B, and C, respectively.

The *ab initio* calculations were performed on different nuclear geometry grids for each set of calculations (i.e., for each strategy A–C), and the grids are described in detail in the supporting information.[48] Briefly, the 3380 strategy A geometries were designed to be global and cover the range: $r_{LiF}=2.0$–$15\,a_0$, $r_{HF}=1.2$–$7.0\,a_0$, and $\theta=45$–$179.99°$, where r_{AB} is the A–B internuclear distance and θ is the Li–F–H bond angle. The 2232 strategy B geometries covered a more limited range: $r_{LiF}=2.0$–$15\,a_0$, $r_{HF}=1.4$–$3.0\,a_0$, and $\theta=45$–$179.99°$. The 1362 strategy C geometries covered the range: $r_{LiF}=2.5$–$15\,a_0$, $r_{HF}=1.4$–$2.6\,a_0$, and $\theta=45$–$179.99°$. Each of these grids was

augmented by several additional calculations to improve the quality of the final fit.

The construction of the final quasidiabatic fit for the MRDCI potential energy surfaces of the $\tilde{X}\,^2A'$ and $\tilde{A}\,^2A'$ states, based on the sequence of three sets of MRDCI calculations described above (strategies A–C), is discussed in Sec. III. In addition to using MRDCI to calculate the adiabatic potential energy surfaces of the LiFH system, the MRDCI method was also used to determine the asymptotic form of the off-diagonal matrix elements of the diabatic Hamiltonian. As explained in Sec. III, the diabatic coupling term U_{12} for the LiFH system is constructed using the following two pieces of information: the minimum energy gaps between the adiabatic potential energy surfaces of the $\tilde{X}\,^2A'$ and $\tilde{A}\,^2A'$ states, extracted from the MRDCI calculations for these states as described above, and the magnitude of the coupling between the lowest two $^1\Sigma^+$ states of the LiF and LiH diatomic fragments.

It is much easier to calculate the diabatic coupling for a diatomic than for a triatomic system, and several methods for calculating a diabatic Hamiltonian for a diatomic molecule have been proposed.[38,49–54] In this work, we used the method proposed by Werner and Meyer,[49] in which information about the off-diagonal matrix element of the diabatic Hamiltonian is determined from the adiabatic states that are to be coupled and the transition dipole moments between them (in our case, the lowest two $^1\Sigma^+$ states of LiF and LiH). In order to be consistent, we used the MRDCI approach in these additional calculations. The basis sets for LiF and LiH were obtained using the basis sets for the Li, F, and H atoms employed in the calculations for the LiFH system. We performed two kinds of calculations. In the first set of calculations, we used three threshold values (0.2, 0.4, and 0.6 μE_h for LiF and 0.001, 0.002, and 0.003 μE_h for LiH) and extrapolated the resulting energies to the $T=0$ limit, as we did in the calculations for LiFH. This gave us information about the entire ground- and excited-state potential energy curves of the LiF and LiH molecules (the $X\,^1\Sigma^+$, $A\,^1\Pi$, $B\,^3\Pi$, $C\,^3\Sigma^+$, and $D\,^1\Sigma^+$ states of LiF and the $X\,^1\Sigma^+$, $A\,^3\Sigma^+$, $B\,^1\Sigma^+$, $C\,^3\Pi$, $D\,^1\Pi$, $E\,^3\Sigma^+$ states of LiH). Information about the ground- and first-excited states was useful in designing the correct asymptotic form of our quasidiabatic fit in the LiF+H and LiH+F channels. The corresponding vertical excitation energies can be found in Tables V and VI.

In the second set of calculations, we used the nonextrapolated MRDCI energies for the lowest two $^1\Sigma^+$ states, obtained in the calculations with $T=0.2$ μE_h for LiF and $T=0.001$ μE_h for LiH, and the corresponding dipole moment functions, i.e., the adiabatic dipole moments in the lowest two $^1\Sigma^+$ states and the transition dipole moment between these states, to construct matrix elements U_{11}, U_{22}, and U_{12} of the diabatic Hamiltonians for LiF and LiH as functions of the internuclear separations. The relevant adiabatic energies and dipole moments were obtained on dense grids of points consisting of 45 Li–F distances, ranging between 1.7 and 31.0 a_0, for LiF, and 41 Li–H distances, ranging between 1.5 and 15.0 a_0, for LiH. The reference spaces included 96 references (128 CSFs) for the LiF molecule and 82 references (82 CSFs) for LiH. In order to improve the accuracy of our description of the U_{11}, U_{22}, and U_{12} diabatic potentials for LiF, for which the coupling is stronger, we uniformly shifted the ionic diabat U_{11} to reproduce the difference between the ionic and covalent diabats, $U_{11}-U_{22}$, at the Li–F separation of 31.0 a_0, that results from the classical Rittner model,[55] i.e.,

$$U_{11}-U_{22}=\mathrm{IP(Li)}-\mathrm{EA(F)}-1/R_{\mathrm{LiF}}-\alpha/(2R_{\mathrm{LiF}}^4), \qquad (22)$$

where α equals the sum of the polarizabilities of Li^+ and F^- (we used the polarizability values reported in Refs. 56 and 57). The resulting diabatic potentials U_{11}, U_{22}, and U_{12} for LiF and the corresponding diabatic potentials for LiH were used to design the U_{12} coupling term of the LiFH system (see Sec. III). The high quality of the diabatic states of LiF, obtained in this work with the Werner–Meyer scheme[49] and by the subsequent shifting of the ionic diabat according to Eq. (22) can be seen by analyzing the results listed in Table VII. The Li–F distance at which the U_{11} and U_{22} diabats cross (the crossing radius R_c), and the separation $\Delta E(R_c)$ between the adiabatic energies of the lowest two $^1\Sigma^+$ states of LiF, obtained by rediagonalizing the diabatic Hamiltonian at $R_{\mathrm{LiF}}=R_c$, compare very well with the empirical estimates of R_c and $\Delta E(R_c)$ provided in Ref. 50.

TABLE VII. The crossing radius R_c and the separation $\Delta E(R_c)$ between the two lowest adiabatic $^1\Sigma^+$ states of LiF at the Li–F separation equal to R_c.

	MRDCI[a]	Empirical[b]
R_c/a_0	13.98	13.72
$\Delta E(R_c)$, eV	0.024	0.021

[a]The nonextrapolated MRDCI calculation without the quasidegenerate Davidson correction (Ref. 46). The crossing radius R_c was obtained by diabatizing the MRDCI adiabatic states using the method of Ref. 49. The separation $\Delta E(R_c)$ was obtained by adjusting the U_{11} (ionic) diabat at $R_{\mathrm{LiF}}=31\,a_0$ to the classical Rittner potential [cf. Eq. (22) and Ref. 55] and rediagonalizing the diabatic Hamiltonian to obtain adiabatic energies. The required values of the ionization potential of Li and electron affinity of F were taken from Ref. 74. The required values of the polarizabilities of Li^+ and F^- were taken from Refs. 56 and 57, respectively.
[b]Reference 50.

III. FIT OF THE LOWEST TWO POTENTIAL ENERGY SURFACES

Fitting the adiabatic *ab initio* energies obtained as described in Sec. II directly would involve fitting the complicated features of the avoided crossing, the saddle-point, and the ground-state van der Waals well to a single functional form. In addition, we would have to calculate the nonadiabatic vector coupling term

$$\mathbf{d}(\mathbf{q})=\langle \tilde{X}\,^2A'|\nabla_{\mathbf{q}}|\tilde{A}\,^2A'\rangle, \qquad (23)$$

where $\mathbf{q}$ is the relevant set of nuclear coordinates, on the dense grid of nuclear geometries used in the calculations for the $\tilde{X}\,^2A'$ and $\tilde{A}\,^2A'$ states. This would considerably increase the cost and complexity of our calculations. Thus, instead of

fitting the adiabatic potential energy surfaces and nonadiabatic coupling term **d**, we fit the surfaces quasidiabatically.[35–44,58–60]

The quasidiabatic electronic states, which formally result from a 2×2 unitary transformation of the adiabatic states, are essentially the covalent and ionic states of a valence-bond model, and their energies are relatively smoothly varying functions of geometry. The quasidiabatic potential energy matrix is written as

$$\mathbf{U}(\mathbf{q})=\begin{pmatrix} U_{11}(\mathbf{q}) & U_{12}(\mathbf{q}) \\ U_{12}(\mathbf{q}) & U_{22}(\mathbf{q}) \end{pmatrix}, \tag{24}$$

where U_{11} are U_{22} are the lower- and higher-energy diabatic surfaces, respectively, in the Li+HF asymptotic valley and the higher- and lower-energy diabatic surfaces, respectively, in the LiF+H valley (the quasidiabatic surfaces cross when all three atoms are interacting). The quasidiabatic surfaces are coupled by a single scalar coupling term U_{12}, which is a function of three internal coordinates of LiFH. By defining the set of coupled surfaces using the quasidiabatic surfaces as in Eq. (24), we also define the adiabatic surfaces and their nonadiabatic coupling **d**. The adiabatic energies are obtained without approximation by diagonalizing Eq. (24), i.e.,

$$V_{1(2)}(\mathbf{q})=\tfrac{1}{2}[U_{11}(\mathbf{q})+U_{22}(\mathbf{q})] \mp\tfrac{1}{2}\sqrt{[U_{22}(\mathbf{q})-U_{11}(\mathbf{q})]^2+4U_{12}^2(\mathbf{q})}, \tag{25}$$

where V_1 and V_2 are the adiabatic $\tilde{X}\,^2A'$ and $\tilde{A}\,^2A'$ states, respectively. The nonadiabatic coupling **d** in Eq. (23) may also be obtained without approximation from the quasidiabatic energies and their gradients.[61]

One disadvantage of using the quasidiabatic representation is that it is not unique. A strict diabatic representation would be one in which all of the components of the vector coupling **d** are zero,[51,54] but such a representation does not exist in general[41,42,58–60] (except for the trivial, nonphysical solution of a basis that is independent of nuclear geometry). Nevertheless, useful approximate diabatic representations (i.e., quasidiabatic representations that are expected to contain the essentially correct physics for most practical dynamics calculations even when the momentum coupling is neglected) may often be defined, either based on smoothness and the incorporation of the geometrical dependencies expected on the basis of an underlying valence bond picture of the electronic structure[29–33,35–40] or based on more mathematical arguments.[41–44,62] In the present work we use the former approach.

As mentioned above, we fit the two lowest-energy adiabatic potential energy surfaces of LiFH to a 2×2 quasidiabatic potential energy matrix, Eq. (24). The details of the functional form and parameters used in the 2×2 LiFH fit are presented in the supporting information.[48] Briefly, our first step towards obtaining an analytic global potential energy surface was to obtain one-dimensional analytic fits for the asymptotic potential energy curves for the diatomic potentials of HF and LiF, in each case with the third atom far away. (Note that the LiH diatomic is not accessible at energies for which the current fit was designed to be useful. We therefore did not include the accurate LiH curve explicitly in the present fit.) The HF curve used in fitting the Li+HF asymptotic potentials was based on the RKR experimental data presented in Ref. 63. The LiF curves for the two lowest states of LiF used to fit the LiF+H asymptotic potential, were based on the diatomic *ab initio* calculations for LiF

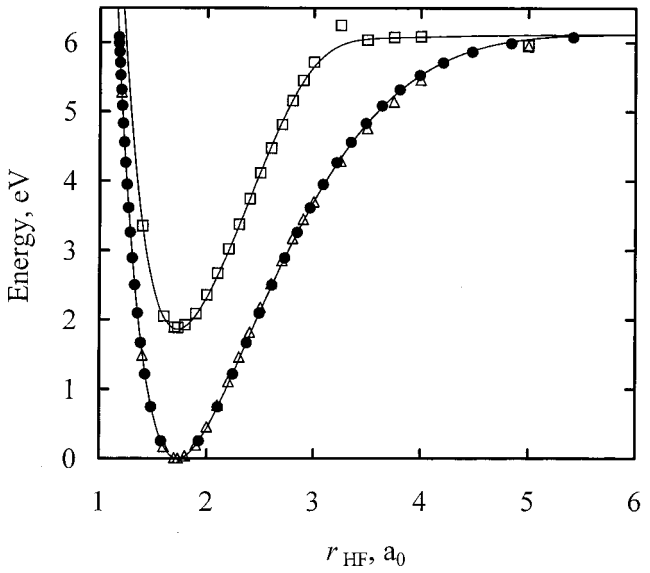

FIG. 1. Asymptotic potential energy curves of LiFH in the Li+HF limit. The analytic fits used in the global fit are shown as solid lines, the solid circles represent the experimental data for HF from Ref. 61 used to obtain the ground-state fit, and the open symbols represent the strategy A *ab initio* data for the ground state (triangles) and excited state (squares) of the LiFH system in the Li+HF limit.

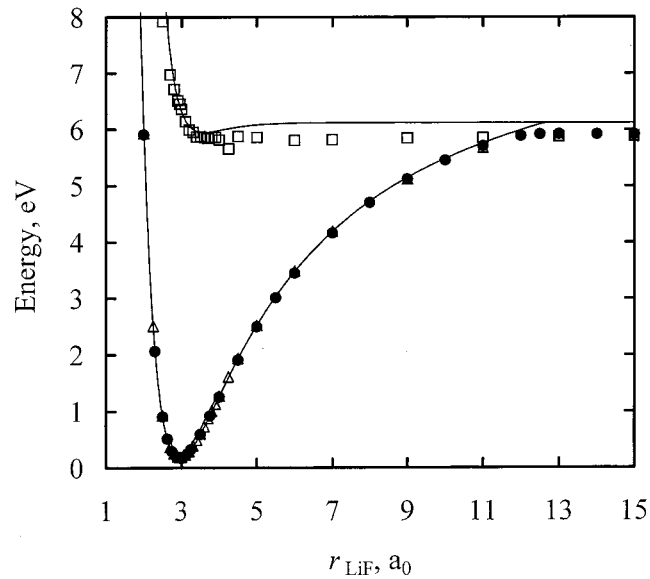

FIG. 2. Asymptotic potential energy curves of LiFH in the H+LiF limit. The analytic fits used in the global fit for LiFH are shown as solid lines, the solid circles represent the highly accurate MRDCI data for the ground state of LiF used to obtain the ground-state fit, and the open symbols represent the strategy A *ab initio* data for the ground state (triangles) and excited state (squares) of the LiFH system in the H+LiF limit.

discussed in Sec. II. Figures 1 and 2 show the fitted Li + HF and H + LiF curves, respectively. Also shown are the experimental and *ab initio* diatomic curves upon which the HF and LiF fits (with the third atom far away) were based, respectively, as well as the strategy A data for these asymptotes (see Sec. II) upon which the global fit for LiFH is based. As seen from Figs. 1 and 2 and as discussed in Sec. II, the global data agree well with the experimental and high-level *ab initio* data.

Also shown in Figs. 1 and 2 are the excited-state *ab initio* data and fits for HF and LiF, respectively, again with the third atom far away. For small r_{HF}, the excited-state fit for the HF curve is equal to the ground-state HF curve shifted to higher energy by the excitation energy of Li (1.848 eV). The full three-body fitting procedure is facilitated when both electronic states go to the same energy when all three atoms are fully separated, and therefore the excited-state HF asymptotic potential was cut off around $r_{\mathrm{HF}}=3.0\ a_0$. The HF asymptotic curves and the ground-state LiF asymptotic curves were not allowed to vary during the remainder of the fitting procedure. The excited-state LiF asymptotic curve is purely repulsive and was allowed to vary during the next step of the fitting procedure.

After determining the asymptotic H + LiF and Li + HF potentials, we developed highly parametrized functional forms for the three-dimensional diabats and the diabatic coupling surface. These functional forms were modeled on our previous fits of the NaFH and NaH_2 systems,[28,33,34] with additional functionality added as demanded by the LiFH *ab initio* data. The U_{11} diabat is relatively featureless and contains only the van der Waals well and the Li($2s$) + HF asymptote. We therefore used a simple sum of diatomic terms to describe U_{11}. The HF potential curve was taken as our fit to the accurate experimental[63] data as discussed above, and two parametrized repulsive curves were used to describe the LiF and LiH diatomic interactions. Flexibility was added to the HF curve in the interaction region. The U_{22} diabat is more complicated since it has two open arrangements, Li($2p$) + HF and LiF + H, as well as a saddle point and a product van der Waals well. We used a highly parametrized generalized LEPS[64–67] function to describe the U_{22} surface. Considerable flexibility in the fit was obtained by using highly modified triplet functions as well as switching functions to add functionality to the singlet curves. See the supporting information[48] for details.

Proper treatment of long-range interactions[68,69] can have a significant impact on observables such as the reaction cross section, as discussed elsewhere.[33] Here, we explicitly include the long-range dispersion and permanent multipole interactions in the U_{11} and U_{22} surfaces. (Note that here we may include the long-range interactions in the quasidiabatic states because the diabatic coupling is nonzero only in the strong interaction region. The quasidiabatic states are therefore equal to the adiabatic states in the regions where the long-range forces are important.) Dispersion and dipole-induced-dipole forces were included in the U_{11} surface for the Li($2s$)–HF interaction and in the U_{22} surface for the Li($2p$)–HF and H–LiF interactions. These interactions are asymptotic to $Q_{\mathrm{A,BC}}^{-6}$ for the interaction A–BC, where $Q_{\mathrm{A,BC}}$ is the distance from the separated atom A to the center of mass of the diatom BC. The Li($2p$) atom has a permanent quadrupole moment, and the U_{22} surface also includes the quadrupole–quadrupole and dipole–quadrupole forces for the Li($2p$)–HF interaction. The dipole–quadrupole and quadrupole–quadrupole interactions are asymptotic to $Q_{\mathrm{Li,HF}}^{-4}$ and $Q_{\mathrm{Li,HF}}^{-5}$, respectively. See the supporting information[48] for further details of the long-range interactions.

The accuracy of the U_{12} surface is critical for obtaining the correct nonadiabatic dynamics, but the adiabatic *ab initio* energies alone do not provide any direct information about the strength of the coupling in the three-body interaction region. We used the following procedure to obtain a reasonable coupling surface. We selected a functional form for U_{12} that behaves asymptotically like the *ab initio* LiF and LiH diabatic coupling curves that we obtained as discussed in Sec. II. We assume that in the interaction region the diabatic coupling will behave similarly to the asymptotic coupling, but the magnitude may be different. The magnitude of the diabatic coupling in the interaction region was estimated from the adiabatic energies near the line of avoided crossing. As seen from Eq. (25), when $U_{11}=U_{22}$, the diabatic coupling U_{12} is given by $(V_2-V_1)/2$. We identified the approximate geometries of the diabatic crossing ($U_{11}=U_{22}$) by using the dense grid of *ab initio* data and locating the line of minimum adiabatic energy gaps at each Li–F–H bond angle. We then estimated the diabatic coupling along this line to be half the adiabatic energy gap and adjusted the functional form of the diabatic coupling to have, as well as possible, the estimated magnitude along the line of avoided crossing at each bond angle. Once the functional form for U_{12} was obtained, cutoff functions were added such that U_{12} vanishes in all asymptotes. This feature does not significantly affect the dynamics, but it greatly simplifies dynamics calculations.

The more than 80 adjustable parameters in the U_{11}, U_{22}, and U_{12} surfaces were optimized simultaneously during the coupled-state triatomic fitting procedure. We used a genetic algorithm[70] to simultaneously fit the parameters of all three surfaces by diagonalizing the quasidiabatic potential energy matrix to obtain the adiabatic energies V_1 and V_2. The parameters were optimized by minimizing the unfitness function f^{-1}, where

TABLE VIII. Mean unsigned error (MUE) in eV of the fitted energies $V_i(\mathbf{R}_j)$ and mean unsigned deviation (MUD) in eV of the *ab initio* data E_{ij} from their mean value for several energy ranges. The mean errors were calculated with unit weight on every point. N_{geom} is the number of geometries for the state indicated that lie within the energy range given in each row.

Surface	Energy range	N_{geom}	MUE	MUD	MUE/MUD
V_1	$E_{1i}<2.5$ eV	1390	0.059	0.543	0.11
	$E_{1i}<2.0$ eV	1323	0.055	0.488	0.11
	$E_{1i}<1.0$ eV	886	0.039	0.275	0.14
	$E_{1i}<0.0$ eV	98	0.017	0.060	0.29
V_2	$E_{2i}<2.5$ eV	1037	0.063	0.294	0.21
	$E_{2i}<2.0$ eV	640	0.044	0.188	0.24
	$E_{2i}<1.8$ eV	436	0.042	0.138	0.31

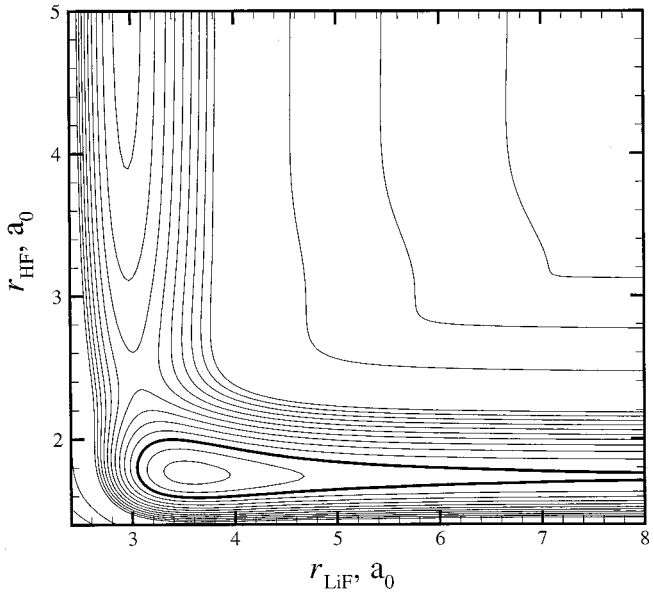

FIG. 3. Contour plot of the fitted ground-state adiabatic surface (V_1) at a Li–F–H bond angle of 107° (the bond angle of the minimum energy of the van der Waals well). The contour spacing is 0.1 eV for energies less than 1.0 eV, and 1.0 eV for energies above 1.0 eV. The contour corresponding to 0.0 eV is shown as a thick solid line. Note: the zero of energy for *all* contour plots in this paper is Li($2s$) infinitely far from HF at its classical equilibrium separation.

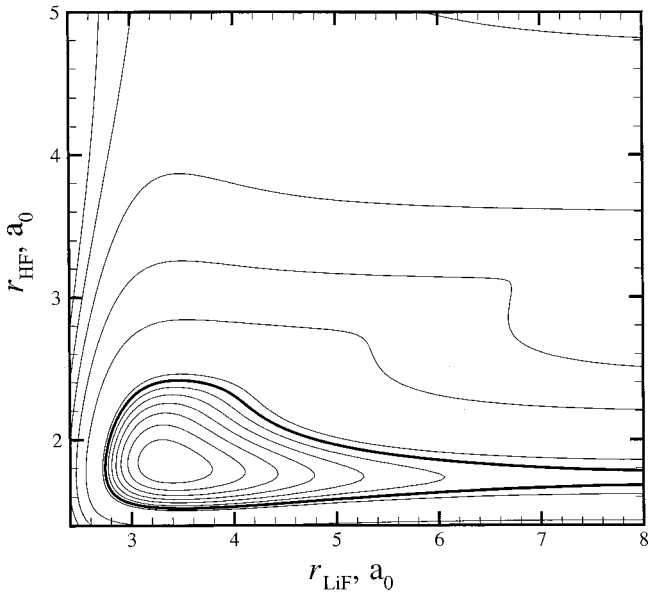

FIG. 5. Contour plot of the fitted first excited-state adiabatic surface (V_2) at a Li–F–H bond angle of 122° (the bond angle of the minimum energy of the exciplex well). The contour spacing is 0.1 eV for energies less than 2.0 eV and 1.0 eV for energies above 2.0 eV. The contour corresponding to 1.9 eV is shown as a thick solid line.

$$f^{-1}=\sum_{i=1}^{2}\sum_{j=1}^{N_i} w_{ij}|E_{ij}-V_i(\mathbf{R}_j)|, \tag{26}$$

where N_i is the number of *ab initio* data points for surface i, $V_i(\mathbf{R}_j)$ is the value of adiabatic potential i for a given set of parameters at geometry $\mathbf{R}_j$, and E_{ij} is the *ab initio* energy of the ith adiabatic surface at geometry $\mathbf{R}_j$. The weights w_{ij} were selected such that the more critical areas (the saddle point, the van der Waals well, the exciplex well, and the seam of avoided crossing) were weighted more heavily than less-critical areas (e.g., the high-energy repulsive walls where two atoms are strongly repelling one another).

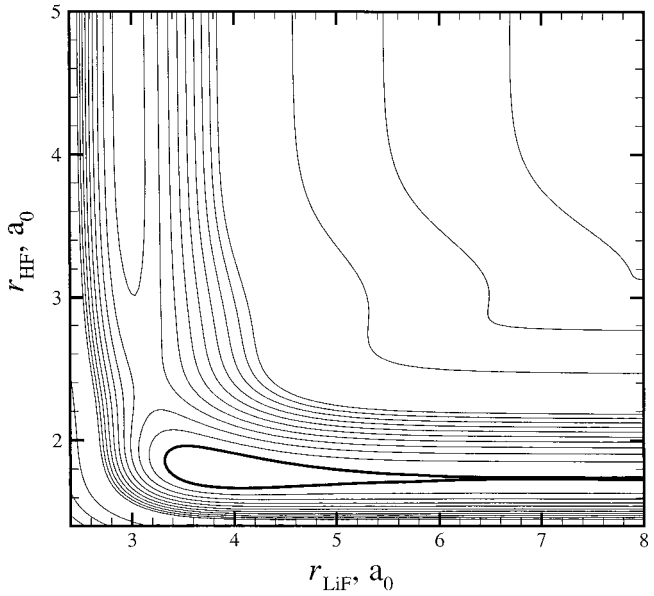

FIG. 4. Contour plot of the fitted ground-state adiabatic surface (V_1) at a Li–F–H bond angle of 72.8° (the bond angle of the saddle point). The contour spacing is 0.1 eV for energies less than 1.0 eV and 1.0 eV for energies above 1.0 eV. The contour corresponding to 0.0 eV is shown as a thick solid line.

We determined the final values of the parameters in two stages. We first obtained the set of parameters which best fits the least accurate global strategy A data. As mentioned in Sec. II, the strategy A data are available over the largest range of geometries (3380 data points). This stage also allowed us to add flexibility to our functional forms as needed. We further refined our fit by allowing subsets of the parameters to vary as we fit V_1 and V_2 to the more accurate strategy B data (2232 data points) for the V_2 surface and the strategy C data (1362 data points) for the V_1 surface. A comparison of the fitted values of V_1 and V_2 for a wide range of nuclear geometries is available as supporting information.[48]

The discussion so far has centered on our most accurate global fit, which we will call surface fit J when we need to distinguish it from the preliminary fit of Ref. 26, which can be called fit H. In some cases one would like to perform dynamics calculations without the added complication of long-range forces (which require longer integration times or longer-ranged grids in dynamics calculations). We therefore also created another surface set, which can be called surface fit JS, that is almost as accurate as surface fit J in the regions where we have *ab initio* data, but has truncated long-range forces. This is fully described in the supporting information.[48] In the rest of the article, *all* discussion refers to surface fit J.

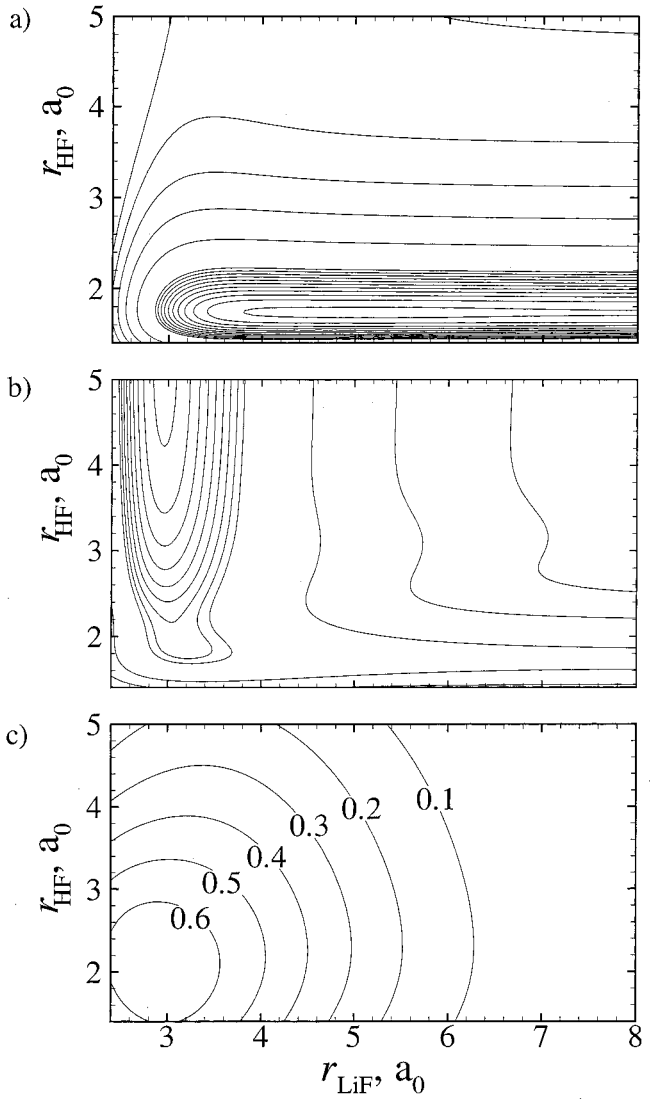

FIG. 6. Contour plots of the (a) U_{11}; (b) U_{22}; and (c) U_{12} quasidiabatic surfaces at a Li–F–H bond angle of 107°. For panels (a) and (b), the contour spacing is 0.1 eV for energies less than 1.0 ev and 1.0 eV for energies above 1.0 eV. For panel (c), the contours are labeled in eV.

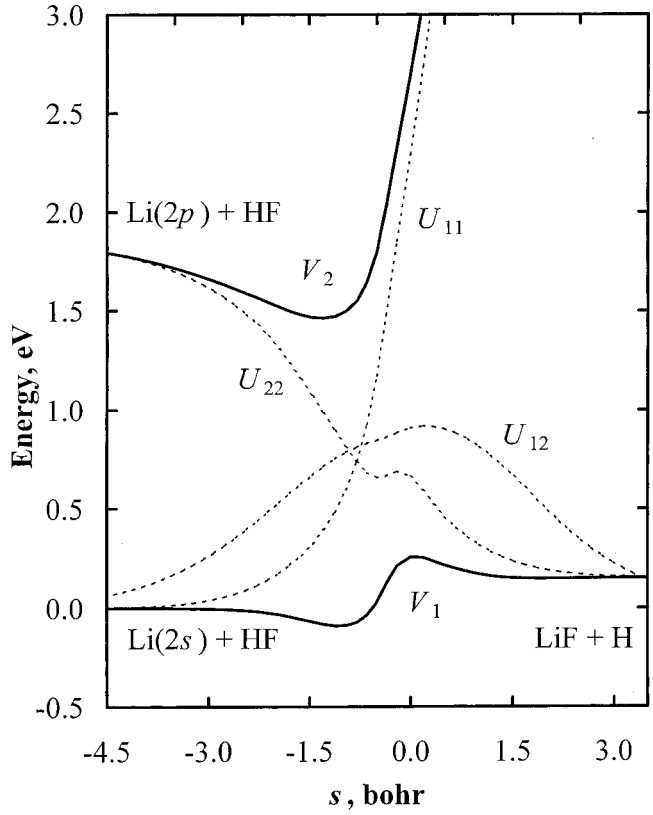

FIG. 7. Adiabatic (thick solid lines) and quasidiabatic (thin dashed lines) energies along the steepest descent path from the saddle point in unscaled rectilinear coordinates (r_{LiF} and r_{HF}) for the ground-state reaction Li($2s$) + HF→LiF+H at a fixed bond angle of $\theta=72.8°$. The distance along the path is the reaction coordinate s.

IV. DISCUSSION OF THE LiFH SURFACES

IV.A. Two lowest-energy states

The mean unsigned error of the fit is tabulated as a function of energy in Table VIII. For energies relative to the dynamics calculations of most interest to us (less than 2.5 eV), the fit agrees with the *ab initio* data to within 0.06 eV (~1.4 kcal/mol) and is even more accurate for lower energies. This is a very good agreement, especially since the *ab initio* data vary over a wide range, as illustrated by the spread of the data, as measured by its unsigned deviation from its mean. The energy of the ground-state van der Waals well is extremely accurate and agrees with the *ab initio* data to within 0.01 eV (0.2 kcal/mol).

Figures 3 and 4 show contour plots of the LiFH ground-state surface at $\theta=107°$ (the angle of the minimum of the ground-state van der Waals complex) and 72.8° (the angle of the ground-state saddle point), respectively, where θ is the Li–F–H bond angle. Figure 5 shows a contour plot of the LiFH first excited-state surface at $\theta=122°$ (the angle of the minimum energy of the exciplex well). The quasidiabatic states U_{11}, U_{22}, and U_{12} are shown in Fig. 6 for the 107° bond angle. Figure 7 shows the adiabatic and diabatic energies along steepest-descent paths from the saddle point for the ground-state Li($2s$)+HF→LiF+H reaction at a fixed Li–F–H bond angle of $\theta=72.8°$. Table IX shows the geometries and the energies of the stationary points, as well as calculations in which the zero-point energy was included by the Morse I approximation[71,72] using the POLYRATE software package.[73]

Table X compares the geometries and energies of stationary points of the fitted adiabatic potential surfaces to those for several other surfaces[4,5,8,11–13] that have appeared in the literature. The critical points of the previous ground-state surfaces agree reasonably well with the fit presented here, and the present fit has the additional advantage over all but one[8] of the previous fits that it also includes the first excited state and over all previous fits that it also includes the electronic state coupling. The excited-state properties of the current fit do not agree well with those reported for the ASP-ALPR fit,[8] as shown in Table X. Specifically, the Li–F–H bond angle of the minimum-energy geometry in the exciplex well for the current fit ($\theta=122°$) differs from the result reported by ASP-ALPR ($\theta=180°$), and the depth of the exci-

TABLE IX. Geometries and energies of the adiabatic stationary points of LiFH as calculated from the global fit. All bond lengths are in bohrs, the Li–F–H angle θ is in degrees, and the energies are in eV.

Feature	r_{LiF}	r_{HF}	r_{LiH}	θ	V_1	V_1+ZPE[a]	V_2	V_2+ZPE[a]
Reactants	⋯	1.73	⋯	⋯	0.000	0.255	1.848	2.099
Reactant vdW well of V_1	3.56	1.76	4.42	107.0	−0.241	0.033	1.244	⋯
Saddle point[b] of V_1	3.10	2.62	3.42	72.8	0.247	0.352	3.227	⋯
Product vdW well of V_1	2.98	3.90	3.94	68.4	0.150	0.242	5.567	⋯
Products	2.96	⋯	⋯	⋯	0.175	0.232	[c]	⋯
Exciplex of V_2	3.34	1.82	4.57	122.	−0.166	⋯	1.214	1.438

[a]The zero-point energy (ZPE) was calculated by treating the normal modes as separable Morse I oscillators (Refs. 71, 72) using the POLYRATE v. 8.5.1 software package (Ref. 73). Zero-point energy is included in one mode for reactants and products, in two modes for the saddle points, and in three modes for the local three-body minima.
[b]Imaginary frequency: $505i$ cm^{-1}.
[c]The product arrangement is not bound on the excited-state surface V_2.

plex well with respect to the Li($2p$)+HF asymptote also differs significantly; we report an exciplex well depth of 0.68 eV, whereas the APS fit reports a well depth of ~0.9 eV.

IV.B. Other excited states

For completeness, we also include contour plots of the *ab initio* data for the second-excited ($\tilde{B}\,^2A''$) and third-excited ($\tilde{C}\,^2A'$) states as Figs. 8 and 9, respectively. Both figures show the *ab initio* data for $\theta=110°$. These two states are degenerate with the $\tilde{A}\,^2A'$ state in the Li+HF limit (the $\tilde{A}\,^2A'$, $\tilde{B}\,^2A''$, and $\tilde{C}\,^2A'$ states correspond to the threefold degenerate $2p\,^2P$ state of the Li atom in the Li+HF limit). To further illustrate the role that these states may play in the dynamics of electronically excited LiFH, Figs. 10 and 11show cuts through the ground-state van der Waals well for $\theta=110°$ and fixed values of r_{HF} and r_{LiF}, respectively. The analytic fit for the ground-state and first-excited states are shown as solid lines, and the *ab initio* data are connected with dashed lines for the excited states that are not included in the analytic fit. The symbols represent the *ab initio* data.

V. SUMMARY AND FORTRAN VERSION

We have presented the results of accurate high-level *ab initio* calculations for the first six states of the LiFH system at a large range of geometries. We have used these data to construct a highly accurate 2×2 quasidiabatic analytic fit to the first two adiabatic potential energy surfaces. The fit explicitly includes long-range interactions and the electronic state coupling. The geometries and energies of the stationary points (the ground-state reactant van der Waals well, the

TABLE X. Comparisons of the geometries and energies of the stationary points on the adiabatic potential surfaces for several fitted LiFH potential energy surfaces.

	Present	CS[a]	CM[b]	ASP-ALPR[c]	PLCP[d]	APLR[e]	BPSB[f]
Reactants							
r_{HF} (a_0)	1.73	1.76	1.73	1.74	1.73	1.74	⋯
V_1 (eV)	0.0	0.0	0.0	0.0	0.0	0.0	⋯
V_2 (eV)	1.85	⋯	⋯	2.05	⋯	⋯	⋯
van der Waals well							
r_{LiF} (a_0)	3.56	3.68	3.59	3.65	⋯	3.55	3.60
r_{HF} (a_0)	1.76	1.78	1.76	1.76	⋯	1.77	1.76
θ (deg)	107	109	114	106	⋯	107	109
V_1 (eV)	−0.24	−0.20	−0.26	−0.29	−0.30	−0.28	−0.25
Saddle point							
r_{LiF} (a_0)	3.10	3.21	3.12	3.20	⋯	3.20	3.14
r_{HF} (a_0)	2.62	2.44	2.48	2.46	⋯	2.46	2.42
θ (deg)	72.8	71	74	73	74	71.4	71.2
V_1(eV)	0.25	0.43	0.34	0.25	0.18	0.23	0.25
Products							
r_{LiF} (a_0)	2.96	3.03	2.95	3.00	2.96	3.00	⋯
V_1 (eV)	0.18	0.13	0.17	0.10	0.15	08	⋯
Exciplex well							
r_{LiF} (a_0)	3.34	⋯	⋯	3.18	⋯	⋯	⋯
r_{HF} (a_0)	1.82	⋯	⋯	1.95	⋯	⋯	⋯
θ (deg)	122.	⋯	⋯	180.	⋯	⋯	⋯
V_2 (eV)	1.21	⋯	⋯	1.16	⋯	⋯	⋯

[a]Reference 4.
[b]Reference 5.
[c]Reference 8.
[d]Reference 11.
[e]Reference 12.
[f]Reference 13.

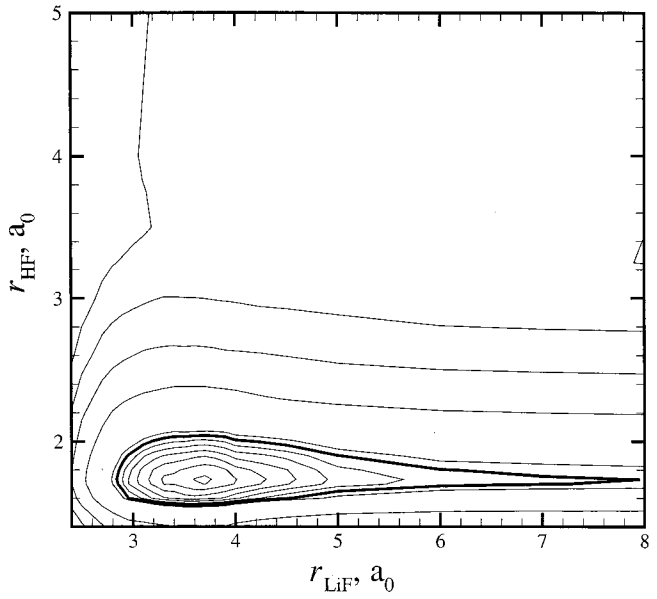

FIG. 8. Contour plot of the *ab initio* data for the second-excited state ($\tilde{B}\,^2A''$) at a Li–F–H bond angle of 110°. The contour spacing is 0.1 eV for energies less than 2.0 eV and 1.0 eV for energies above 2.0 eV. The contour corresponding to 1.9 eV is shown as a thick solid line.

ground-state saddle point, the ground-state product van der Waals well, and the exciplex well) agree well with other (less complete) fits that have been presented in the literature. The surface set presented in this paper should be useful for dynamical modeling of the global electronically nonadiabatic dynamics in both reactive and nonreactive processes.

A FORTRAN copy of the fitted potential matrix is available in the POTLIB library.[77]

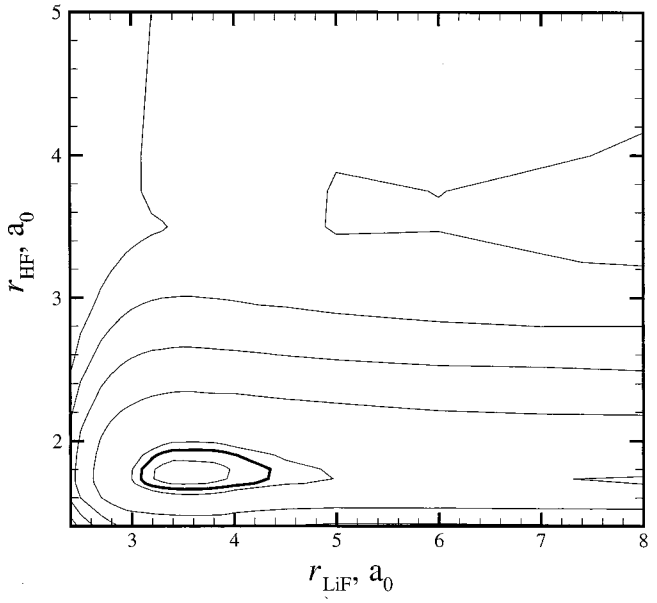

FIG. 9. Contour plot of the *ab initio* data for the third-excited state ($\tilde{C}\,^2A'$) at a Li–F–H bond angle of 110°. The contour spacing is 0.1 eV for energies less than 2.0 eV and 1.0 eV for energies greater than 2.0 eV. The contour corresponding to 1.9 eV is shown as a thick solid line.

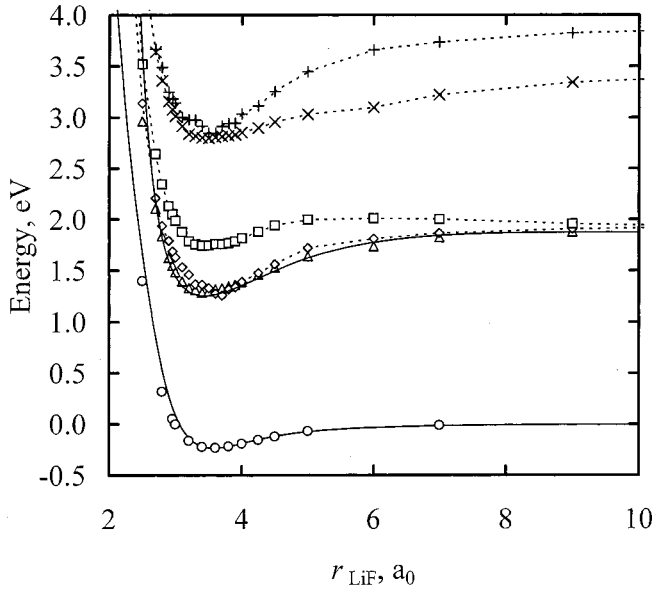

FIG. 10. Cut along r_{LiF} through the minimum of the ground-state van der Waals well at a fixed Li–F–H bond angle of 110° with r_{HF} fixed at 1.73 a_0. The analytic fits for the two lowest-energy states are shown as solid lines. The *ab initio* data are shown as symbols, where the circles represent the $\tilde{X}\,^2A'$ state, triangles represent the $\tilde{A}\,^2A'$ state, diamonds represent the $\tilde{B}\,^2A''$ state, squares represent the $\tilde{C}\,^2A'$ state, "×" represent the $\tilde{D}\,^2A'$ state, and "+" represent the $\tilde{E}\,^2A''$ state. The symbols are connected by dashed lines for the states not included in the analytic fits.

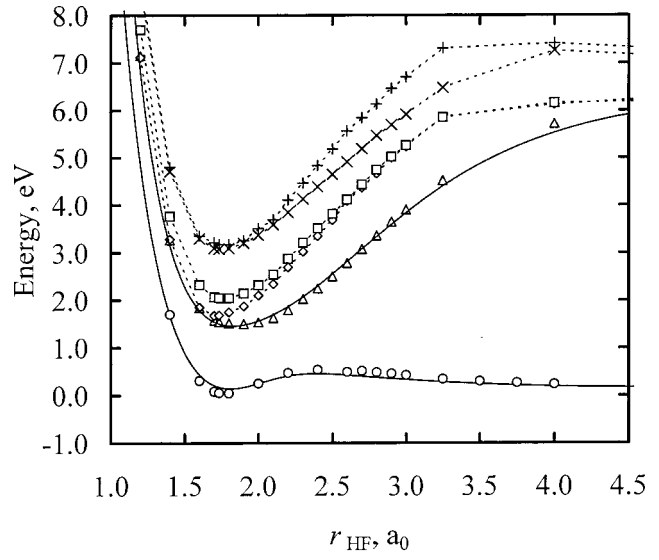

FIG. 11. Cut along r_{HF} through the minimum of the ground-state van der Waals well at a fixed Li–F–H bond angle of 110° with r_{LiF} fixed at 2.96 a_0. The analytic fits for the two lowest-energy states are shown as solid lines. The *ab initio* data are shown as open symbols, where the circles represent the $\tilde{X}\,^2A'$ state, triangles represent the $\tilde{A}\,^2A'$ state, diamonds represent the $\tilde{B}\,^2A''$ state, squares represent the $\tilde{C}\,^2A'$ state, "×" represent the $\tilde{D}\,^2A'$ state, and "+" represent the $\tilde{E}\,^2A''$ state. The symbols are connected by dashed lines for the states not included in the analytic fits.

ACKNOWLEDGMENTS

This work was supported in part by the National Science Foundation under Grant No. CHE00-92019 and by the Michigan State University Intramural Research Grant Program.

[1] W. A. Lester, Jr. and M. Krauss, J. Chem. Phys. **52**, 4775 (1970).
[2] G. G. Balint-Kurti and R. N. Yardley, Faraday Discuss. Chem. Soc. **62**, 77 (1977).
[3] Y. Zeiri and M. Shapiro, Chem. Phys. **31**, 217 (1978); M. Shapiro and Y. Zeiri, J. Chem. Phys. **70**, 5264 (1979).
[4] M. M. L. Chen and H. F. Schaefer III, J. Chem. Phys. **72**, 4376 (1980).
[5] S. Carter and J. N. Murrell, Mol. Phys. **41**, 567 (1980).
[6] A. Laganà and E. Garcia, THEOCHEM **16**, 91 (1984); E. Garcia and A. Laganà, Mol. Phys. **52**, 1115 (1984); V. Aquilanti, A. Laganà, and R. D. Levine, Chem. Phys. Lett. **158**, 87 (1989); A. Laganà, G. O. d. Aspuru, and E. Garcia, J. Chem. Phys. **108**, 3886 (1998).
[7] M. Paniagua and A. Aguado, Chem. Phys. **134**, 287 (1989); A. Aguado and M. Paniagua, J. Chem. Phys. **96**, 1265 (1992); C. Suárez, A. Aguado, and M. Paniagua, Chem. Phys. **178**, 357 (1993); C. Suárez, A. Aguado, C. Tablero, and M. Paniagua, Int. J. Quantum Chem. **52**, 935 (1994).
[8] A. Aguado, C. Suárez, and M. Paniagua, Chem. Phys. **201**, 107 (1995); A. Aguado, M. Lara, M. Paniagua, and O. Roncero, J. Chem. Phys. **114**, 3440 (2001).
[9] O. N. Ventura, Mol. Phys. **89**, 1851 (1996).
[10] A. Laganà, O. Gervasi, and E. García, Chem. Phys. Lett. **143**, 174 (1988).
[11] G. A. Parker, A. Laganà, S. Crocchianti, and R. T Pack, J. Chem. Phys. **102**, 1238 (1995).
[12] A. Aguado, M. Paniagua, M. Lara, and O. Roncero, J. Chem. Phys. **106**, 1013 (1997); **107**, 10085 (1997).
[13] R. Burcl, P. Piecuch, V. Špirko, and O. Bludský, Int. J. Quantum Chem. **80**, 916 (2000).
[14] C. H. Becker, P. Casavecchia, P. W. Tiedeman, J. J. Valentini, and Y. T. Lee, J. Chem. Phys. **73**, 2833 (1980).
[15] R. B. Walker, Y. Zeiri, and M. Shapiro, J. Chem. Phys. **74**, 1763 (1981).
[16] J. M. Alvariño, M. L. Hernández, E. Garcia, and A. Laganà, J. Chem. Phys. **84**, 3059 (1986); A. Laganà, E. Garcia, and O. Gervasi, *ibid.* **89**, 7238 (1988); A. Laganà, X. Giménez, E. Garcia, and O. Gervasi, Chem. Phys. Lett. **176**, 280 (1991); A. Laganà, G. O. d. Aspuru, A. Aguilar, X. Giménez, and J. M. Lucas, J. Phys. Chem. **99**, 11696 (1995); J. M. Alvariño, V. Aquilanti, S. Cavalli, S. Crocchianti, A. Laganà, and T. Martinez, J. Chem. Phys. **107**, 3339 (1997); A. Laganà, A. Bologna, and S. Crocchianti, Phys. Chem. Chem. Phys. **2**, 535 (2000).
[17] G. G. Balint-Kurti, F. Gögtas, S. P. Mort, A. R. Offer, A. Laganà, and O. Gervasi, J. Chem. Phys. **99**, 9567 (1993); F. Gögtas, G. G. Balint-Kurti, and A. R. Offer, *ibid.* **104**, 7927 (1996).
[18] M. Hoffmeister, R. Schleysing, F. Steinkemeier, and H. J. Loesch, J. Chem. Phys. **90**, 3528 (1989); H. J. Loesch, E. Stenzel, and B. Wüstenbecker, *ibid.* **95**, 3841 (1991); H. J. Loesch and F. Steinkemeier, J. Chem. Phys. **98**, 9570 (1993); **99**, 9598 (1993); H. J. Loesch, A. Ramscheid, E. Stenzel, F. Steinkemeier, and B. Wuestenbecker, in *Physics of Electronic and Atomic Collisions*, edited by W. R. MacGilliuray, I. E. McCarthy, and M. C. Staudagi (Hilger, Bristol, 1992), p. 579.
[19] M. Baer, H. J. Loesch, H.-J. Werner, and I. Last, Chem. Phys. Lett. **291**, 372 (1994); M. Baer, I. Last, and H. J. Loesch, J. Chem. Phys. **101**, 9648 (1994).
[20] G. Villani and R. Wallace, Acta Chim. Hung. **131**, 167 (1994); ACH-Models Chem. **131**, 167 (1994).
[21] W. Zhu, D. Wang, and J. Z. Zhang, Theor. Chem. Acc. **96**, 31 (1997).
[22] M. Paniagua, A. Aguado, M. Lara, and O. Roncero, J. Chem. Phys. **109**, 2971 (1998); **111**, 6712 (1999).
[23] M. Lara, A. Aguado, O. Roncero, and M. Paniagua, J. Chem. Phys. **109**, 9391 (1998).
[24] F. J. Aoiz, M. T. Martinez, M. Menéndez, V. S. Rábanos, and E. Verdasco, Chem. Phys. Lett. **299**, 25 (1999).
[25] F. J. Aoiz, E. Verdasco, V. S. Rábanos, H. J. Loesch, M. Menéndez, and F. Steinkemeier, Phys. Chem. Chem. Phys. **2**, 541 (2000).
[26] A. W. Jasper, M. D. Hack, A. Chakraborty, D. G. Truhlar, and P. Piecuch, J. Chem. Phys. **115**, 7945 (2001).
[27] C. Sanz, O. Roncero, M. Paniagua, and A. Aguado, Chem. Phys. Lett. **351**, 295 (2002).
[28] A. J. Hudson, H. B. Oh, J. C. Polanyi, and P. Piecuch, J. Chem. Phys. **113**, 9897 (2000). A. J. Hudson and J. C. Polanyi (personal communication).
[29] J. C. Tully, J. Chem. Phys. **59**, 5122 (1993).
[30] B. C. Garrett and D. G. Truhlar, *in Theory of Scattering: Papers in Honor of Henry Eyring* (Theoretical Chemistry, Vol. 6), edited by D. Henderson (Academic, New York, 1981), Part A, p. 216.
[31] D. G. Truhlar, J. W. Duff, N. C. Blais, J. C. Tully, and B. C. Garrett, J. Chem. Phys. **77**, 764 (1982); N. C. Blais, D. G. Truhlar, and B. C. Garrett, *ibid.* **78**, 2956 (1983).
[32] P. Halvick and D. G. Truhlar, J. Chem. Phys. **96**, 2895 (1992).
[33] M. D. Hack and D. G. Truhlar, J. Chem. Phys. **110**, 4315 (1999).
[34] M. S. Topaler, D. G. Truhlar, X. Y. Chang, P. Piecuch, and J. C. Polanyi, J. Chem. Phys. **108**, 5349 (1998); **108**, 5378 (1998).
[35] T. F. O'Malley, Adv. At. Mol. Phys. **7**, 223 (1971).
[36] V. Sidis and H. Lefebvre-Brion, J. Phys. B **4**, 1040 (1971).
[37] S. A. Evans, J. S. Cohen, and N. F. Lane, Phys. Rev. A **4**, 2235 (1971).
[38] R. W. Numrich and D. G. Truhlar, J. Phys. Chem. **79**, 2745 (1975).
[39] A. Macias and A. Riera, J. Phys. B **11**, L489 (1978).
[40] V. Sidis, Adv. Chem. Phys. **82**, 73 (1992).
[41] T. C. Thompson, D. G. Truhlar, and C. A. Mead, J. Chem. Phys. **82**, 2392 (1985).
[42] T. Pacher, L. S. Cederbaum, and H. Köppel, Adv. Chem. Phys. **84**, 293 (1993).
[43] V. M. García, M. Reguero, R. Caballol, and J. P. Malrieu, Chem. Phys. Lett. **281**, 161 (1997).
[44] G. J. Atchity and K. Ruedenberg, Theor. Chem. Acc. **97**, 47 (1997).
[45] R. J. Buenker and S. D. Peyerimhoff, Theor. Chim. Acta **35**, 33 (1974); **39**, 217 (1975); P. J. Bruna and S. D. Peyerimhoff, Adv. Chem. Phys. **67**, 1 (1987).
[46] J. Paldus, in *New Horizons of Quantum Chemistry*, edited by P. O. Löwdin and B. Pullman (Reidel, Dordrecht, 1983), p. 31; R. J. Buenker and S. D. Peyerimhoff, *ibid.*, p. 183; P. J. Bruna, S. D. Peyerimhoff, and R. J. Buenker, Chem. Phys. Lett. **72**, 278 (1980); K. Jankowski, L. Meissner, and J. Wasilewski, Int. J. Quantum Chem. **28**, 931 (1985).
[47] R. Krishnan, J. S. Binkley, R. Seeger, and J. A. Pople, J. Chem. Phys. **72**, 650 (1980).
[48] See EPAPS Document No. E-JCPSA6-116-312216 for supporting information including the nuclear geometry grids for the *ab initio* calculations, the functional forms and FORTRAN programs for the analytic LiFH potential energy matrices, and a selection of the *ab initio* and fitted energies. This document may be retrieved via the EPAPS homepage (http://www.aip.org/pubserv/epaps.html) or from ftp.aip.org in the directory /epaps/. See the EPAPS homepage for more information.
[49] H.-J. Werner and W. Meyer, J. Chem. Phys. **74**, 5802 (1981).
[50] R. Grice and D. R. Herschbach, Mol. Phys. **27**, 159 (1974).
[51] F. T. Smith, Phys. Rev. **179**, 111 (1969).
[52] S. A. Adelman and D. R. Herschbach, Mol. Phys. **27**, 159 (1974).
[53] L. R. Kahn, P. J. Hay, and I. Shavitt, J. Chem. Phys. **61**, 3530 (1974).
[54] M. Baer, Mol. Phys. **40**, 1011 (1980).
[55] E. S. Rittner, J. Chem. Phys. **19**, 1030 (1951).
[56] P. W. Fowler and P. A. Madden, Phys. Rev. B **29**, 1035 (1984).
[57] S. A. Kucharski, Y. S. Lee, G. D. Purvis III, and R. J. Bartlett, Phys. Rev. A **29**, 1619 (1984).
[58] A. D. McLachlan, Mol. Phys. **4**, 417 (1961).
[59] C. A. Mead and D. G. Truhlar, J. Chem. Phys. **77**, 6090 (1982).
[60] C. A. Mead, J. Chem. Phys. **78**, 807 (1983).
[61] M. D. Hack, A. W. Jasper, Y. L. Volobuev, D. W. Schwenke, and D. G. Truhlar, J. Phys. Chem. A **103**, 6309 (1999).
[62] H. Nakamura and D. G. Truhlar, J. Chem. Phys. **115**, 10353 (2001).
[63] G. Di Lonardo and A. E. Douglas, Can. J. Phys. **51**, 434 (1973); J. A. Coxon and P. G. Hajigeorgiou, J. Mol. Spectrosc. **142**, 254 (1990).
[64] S. Sato, J. Chem. Phys. **23**, 2465 (1955).
[65] J. K. Cashion and D. R. Herschbach, J. Chem. Phys. **40**, 2358 (1964).
[66] K. J. Laidler and J. C. Polanyi, Prog. React. Kinet. **3**, 1 (1965).
[67] P. J. Kuntz, E. M. Nemeth, J. C. Polanyi, S. D. Rosner, and C. E. Young, J. Chem. Phys. **44**, 1168 (1966).
[68] J. O. Hirschfelder, C. F. Curtiss, and R. B. Bird, *Molecular Theory of Gases and Liquids*, corrected printing (Wiley, New York, 1964).
[69] G. C. Maitland, M. Rigby, E. B. Smith, and W. A. Wakeham, *Intermolecular Forces: Their Origin and Determination*, corrected printing (Clarendon, Oxford, 1987); P. Piecuch, in *Molecules in Physics, Chemistry and Biology*, edited by J. Maruani (Kluwer, Dordrecht, 1988), Vol. 2, p. 417.
[70] Genetic algorithm calculations were carried out using the program

FORTRAN GA, version 1.6.4, as described in D. L. Carroll, AIAA J. **34**, 338 (1996).
[71] E. B. Wilson, J. C. Decius, and P. C. Cross, *Molecular Vibrations* (McGraw-Hill, New York, 1955).
[72] A. D. Isaacson and D. G. Truhlar, J. Chem. Phys. **76**, 1380 (1982).
[73] J. C. Corchado, Y.-Y. Chuang, P. L. Fast *et al.*, POLYRATE-version 8.5.1, University of Minnesota, Minneapolis, 2000.
[74] *CRC Handbook of Chemistry and Physics*, 77th ed., edited by D. R. Lide (CRC, Boca Raton, 1996).
[75] K. P. Huber and G. Herzberg, *Molecular Spectra and Molecular Structure*, Vol. 4, Constants of Diatomic Molecules (Van Nostrand Reinhold, New York, 1979).
[76] M. Bettendorf, R. J. Buenker, S. D. Peyerimhoff, and J. Römelt, Z. Phys. A **304**, 125 (1982).
[77] R. J. Duchovic, Y. L. Volobuev, G. C. Lynch, D. G. Truhlar, T. C. Allison, A. F. Wagner, B. C. Garrett, J. C. Corchado, and A. W. Jasper, POTLIB-online, http://comp.chem.umn.edu/potlib/